# SIMPLIFIED FRACTURE RESISTANCE ASSESSMENT IN SHIP STRUCTURE

***Y. Quéméner*† *C.H. Huang and C.F. Lee***

Research department, China Corporation Register of Shipping (CR)
Taipei, Taiwan
*Keywords: Fracture, Longitudinal Member, FAD, CTOD*

## ABSTRACT

This study investigates the fracture failure of ship longitudinal members, in which a crack has propagated by fatigue. During the ship life, some fatigue cracks may propagate till lengths that can be critical in view of the fast fracture, when the ship meets extreme sea conditions. This critical crack length characterizes the fracture resistance of a structure. This study proposes a simplified approach to evaluate the critical crack length. Specifically, this study employs the failure assessment diagram methodology to assess the conditions of failure at the crack tip. Based on two crack configurations, this study establishes the analytical formulations of the crack-tip condition that are regressed using finite element analyses. The material toughness is expressed in terms of crack-tip opening displacement. This simplified approach can thus rapidly compute the failure stress of cracked longitudinal members as a function of the crack length. The critical crack lengths corresponding to the maximum longitudinal stresses derived from long-term extreme loads can thus be determined. For the "Capesize" bulk carrier considered in this study, the critical crack lengths are found to be very large. So,the fracture resistance is found satisfactory.

## INTRODUCTION

During the ship's lifetime, fatigue cracks may initiate in the ship's structure. These cracks can propagate to a length that can be critical in view of the fast fracture when the ship encounters extreme loading conditions. This critical crack length characterizes the fracture resistance of the structural members. It is well accepted that ship design and fabrication provides sufficient fracture resistance to the structure. The IACS [1] states that, in ships, inherent redundancy prevents the local loss of a structural member from immediately endangering the global structural integrity. Steel toughness is also finely controlled to ensure that fatigue cracks do not result in extensive brittle fractures, as it has occurred in the past for the Liberty ships. However, the newly adopted goal based ship construction standards (GBS) [2] provide that the actual redundancy in ship design must be demonstrated. Therefore, this study proposes a quantitative assessment of the fracture resistance in ship.

On a microscopic scale, Anderson [3] describes the ductile fracture in three stages as shown in Fig. 1(a) the void nucleation, (2) the void growth, (3) the void coalscence or crack growth. Amongst others, the Gurson model initially proposed by Gurson[4] and successively completed by Thomason[5] and Zhang[6], is often employed in Finite Element Analyses (FEA) to reproduce finely this three-stages fracture behaviour for a given material. However, this kind of material behaviour is complicated to implement in a finite element method and it requires numerous material data for its calibration. For this study, simplified approaches are preferred to evaluate the fracture resistance of longitudinal members that are structural components where fatigue cracks are very likely to occur. This study focuses on the fracture resistance at the onset of fracture, and ignores the subsequent crack growth resistance behaviour.

Researchers have proposed various approaches to address this problem. Dinovitzer et al. [7] analyzed the fracture toughness of typical longitudinal members in the

† Corresponding author(yann.quemener@crclass.org.tw)

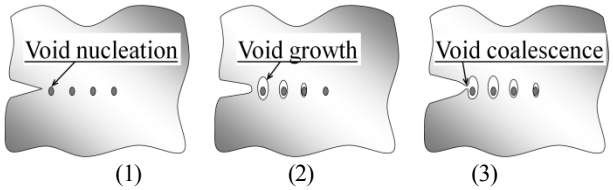


Fig.1 Three-stages ductile fracture behaviour

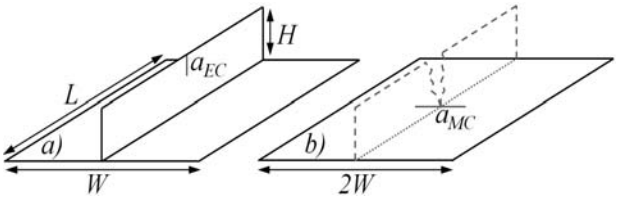


Fig. 2 Stiffened plate element including a) an edge crack in the stiffener, b) a middle crack in the plate

ship structure using the failure assessment diagram (FAD) methodology of the British Standard[8]. The European fitness-for-service network (FITNET)[9] developed also a structural integrity assessment procedure (SINTAP) to determine the significance of cracks in terms of fracture.

This article consists of three sections. The first section presents the scope of the study. The second section establishes, for various crack configurations, the analytical expressions of the crack-tip condition. Finally, the third section evaluates the fracture resistance.

## SCOPE OF THE STUDY

### 1. Cases of study

The ship considered in this study is a Capesize bulk carrier in full loading condition. Two longitudinal members in the midship area have been selected from the deck and the bottom region. Indeed, the high level of stresses in these regions leads to greater material toughness requirements [10] than in other locations. The considered longitudinal member called a Stiffened Plate Element (SPE) by the ultimate capacity assessment methodology of IACS [1], consists of a stiffener and its attached plating. This study represents the stiffener as a flat bar. Figure 2 shows the SPE geometry, where $H$ is the stiffener's web height, $W$ is the stiffener's spacing, and $L$ is the longitudinal member's span between two transverse primary members.

Table 1 presents the dimensions and properties of the two longitudinal members picked up from the deck ($SPE_{Deck}$) and bottom ($SPE_{Bottom}$) regions. Because large fatigue cracks are more likely to occur in the end of the ship's life, this study considers that the SPE are corroded to the net thickness.

Table 1 SPE dimensions and properties

| Properties (Unit) | Symbols | $SPE_{Deck}$ | $SPE_{Bottom}$ |
|---|---|---|---|
| Web height (mm) | $H$ | 370 | 320 |
| Web thickness* (mm) | $t_w$ | 9 | 9 |
| Stiffener spacing (mm) | $W$ | 880 | 850 |
| Plating thickness* (mm) | $t_p$ | 17 | 18 |
| Length (mm) | $L$ | 5700 | 2850 |
| Steel grade (-) | - | EH36 | AH32 |
| Yield stress ($N/mm^2$) | $\sigma_Y$ | 355 | 315 |
| Young modulus ($N/mm^2$) | $E$ | 210000 | |
| Poison coefficient (-) | $\nu$ | 0.3 | |

* Net thickness

The studied crack initiates from the stiffener's free edge and grows by fatigue through the web height till the fillet weld. Then, it propagates through the plating. So, this study considers two crack configurations:

- An edge crack propagates from the stiffener's free edge through the web height, whereas the plating remains uncracked. This crack configuration is called a stiffened plate element including an edge crack in the stiffener. Fig. 2a shows a representation of this crack configuration where $a_{EC}$ is the edge crack length.
- The previously fractured stiffener generates a hotspot at the connection with the plating. Therefore, a fatigue crack is expected to appear at this location. This crack configuration is called a stiffened plate element including a middle crack in the plating. Fig. 2b shows this crack configuration where $a_{MC}$ is the full length of the middle crack.

The middle crack in the plating affects the entire width of the plating between the two adjacent stiffeners. Therefore, for the middle crack configuration, the plating width corresponds to twice the stiffener spacing ($2W$; see Fig. 2b), whereas a plating width corresponding to one time the stiffener spacing ($W$; see Fig. 2a) has been retained for the edge crack configuration.

Under the action of the hull girder vertical bending moment, the hull bending curvature imposes a uniform longitudinal displacement ($\Delta$) on the SPEs with an amplitude directly proportional to its vertical location in the hull cross- section. The material behaviour is set as linear-elastic with an elasticity modulus ($E$), leading to the expression of the longitudinal stress in the SPE in Eq. (1).

$$\sigma_{SPE} = \frac{\Delta}{L} E \tag{1}$$

This study assesses the condition of fracture for those longitudinal members.

## 2. Fracture mechanics

For this study, a simplified criterion to determine the condition of failure is preferred to complex simulations including a specific material failure criterion like the one formulated by Gurson [4], Thomason [5] and Zhang [6]. Indeed, on an engineering point of view, it is much more practical to use a macroscopic dedicated parameter characterizing the fracture even if its application range is limited.

The assessment of the conditions of failure can thus be carried out by comparing two parameters characterizing the fracture. On one side, an applied crack driving force can be evaluated as a function of the applied loads and the geometry of a cracked structure. On the other side, the material toughness can be measured by specimens testing. If the applied crack driving force is greater than the material toughness, the conditions of failure by fracture are satisfied. However, to be comparable, the applied crack driving force and the material toughness must be evaluated based on common assumptions. If this requirement is satisfied, the material toughness obtained from specimens testing is said "transferrable" to the structure.

Usually, two fields of the fracture mechanics are identified for the formulation of parameters characterizing the fracture: 1) the linear-elastic fracture mechanics (LEFM) and 2) the elastic-plastic fracture mechanics (EPFM). The LEFM theory, which is governed by brittle fracture, is reasonably well established, and the stress intensity factor (SIF or K) approach is the most widely employed (e.g.: fatigue crack propagation assessment). However, the steel employed in ship construction is carefully controlled to ensure that fractures occur in a ductile manner. The ductile fracture cannot be assessed accurately by methods purely based on LEFM theory. Thus, some situations require the use of the EPFM using approaches such as the crack-tip opening displacement (CTOD). The applicability of each field of the fracture mechanic is not clearly defined. Thus, a methodology such as the Failure Assessment Diagram (FAD) is a very practical approach because it encompasses the full range of fracture behaviour.

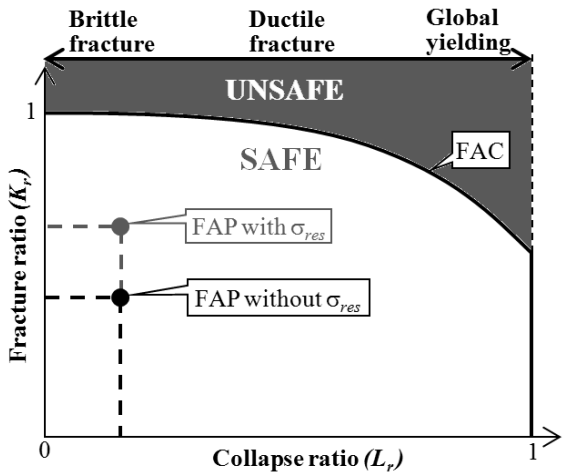


Fig. 3 Failure assessment diagram

## 3. Failure Assessment Diagram

This study is based on the FAD methodology proposed by the British Standard BS7910 [8]. A sounder theoretical background of this approach can be found in [3]. The British Standard proposes three levels of fracture assessment. The choice of the level depends on the amount of input data available and the desired degree of precision of the results. This study uses the "Level 2", defined as the "normal assessment".

The failure assessment diagram principle is based on the interaction between fracture and collapse in a structural component including a crack. Figure 3 presents the failure assessment diagram corresponding to the Level 2.

In the ordinate, the fracture ratio ($K_r$) is the ratio of the applied crack driving force to the fracture toughness of the material. In the abscissa, the collapse ratio ($L_r$) is the ratio of the applied load to the limit load of the structural member.

The failure assessment curve (FAC) represents the predicted limit conditions of the modes of failure, from a brittle to a ductile fracture. Eq. (2) provides the Level-2's FAC expression for $L_r$ from zero till unity. If $L_r$ is greater than unity, $K_r$ is simply set to zero, because this study does not consider the failure by collapse that occurs beyond $L_r$=1.

$$K_r = \left(1 - 0.14L_r^2\right) \cdot \left[0.3 + 0.7\exp\left(-0.65L_r^6\right)\right] \quad (2)$$

A failure assessment point (FAP) can be determined for a given loaded cracked component. If the FAP is included in the area below the FAC (see Fig.3), the considered component is not supposed to fail. An FAP above the FAC represents an unacceptable level of crack which may cause the component failure. In addition, an FAP close to the vertical axis means that the potential fracture is brittle. However, an FAP in the vicinity of a collapse ratio equal to unity indicates that the potential failure is characterized by the global yielding of the considered structural member.

Fig. 4 presents the flowchart of the FAP evaluation procedure. This diagram shows clearly the interest of such a method since the condition of failure can be expressed by a unique combination of applied stress and fatigue crack length. In addition, the material toughness data are easily available.

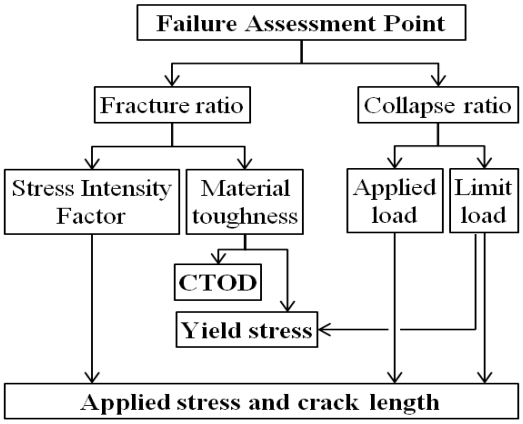

Fig. 4 FAP evaluation flowchart

The fracture ratio expression (see Eq. (3)) is a ratio of the crack driving force represented by the Mode I stress intensity factor ($K_I$) to the material toughness $K_{mat}$, which is derived from the measured CTOD ($\delta_{mat}$).

$$K_r = \frac{K_I}{K_{mat}} = \sqrt{\frac{K_I^2}{X \cdot \sigma_Y \cdot \delta_{mat} \cdot E'}} \tag{3}$$

where $\sigma_Y$ is the material yield stress and $E'$ is the elastic modulus corrected for constraint conditions ($E'=E$ for plane stress, $E'=E/(1-\nu^2)$ for plane strain). The term $X$ is set to 1 as proposed by the British Standard [8] for the case in which $X$ is not quantified by structural analyses. Eq. (4) defines the stress intensity factor ($K_I$).

$$K_I = \sigma \cdot Y \sqrt{\pi a} \tag{4}$$

where $\sigma$ is the applied stress, $Y$ is a dimensionless function related to the crack configuration, and $a$ is the crack length.

Eq. (5) provides the collapse ratio expression.

$$L_r = \frac{P}{P_0} \tag{5}$$

where $P$ is the applied load and $P_0$ is the limit load at which the cracked structural member's yield strength is reached.

Then, the FAD approach classifies stresses based on their nature. The primary stresses $\sigma_p$ are defined as the loads applied to the structure, whereas other stresses, including the residual stress, coming from the fabrication process, are categorized as secondary stresses $\sigma_s$. A significant property of secondary stresses is that they cannot by themselves cause plastic collapse because they arise from stress/displacement limited phenomena. However, they contribute to the severity of the local condition at the crack tip. Their contribution adds to the primary stress in the $K_I$ expression (see Eq. (3)) by replacing $\sigma$ with $\sigma_p+\sigma_s$. Fig.3 presents the effect of the residual stress on the FAP.

Finally, if the structure is loaded with a combination of primary and secondary stresses, the resulting plasticity effects cannot be evaluated by a simple linear addition of the effects resulting from the two independent stress systems. The FAD includes a term $\rho$ to be added to the fracture ratio, that covers the interaction between these two stress systems. The British Standard [8] proposes a simplified formulation of $\rho$ when secondary loads are small, as given in Eq. (6).

$$\text{IF } \chi = K_I^{\,s} / \left(K_I^{\,p} / L_r\right) < 4 \text{, then} \quad \begin{cases} \rho = \rho_1 & \text{for } L_r \le 0.8 \\ \rho = 4 \cdot \rho_1 \cdot (1.05 - L_r) & \text{for } 0.8 < L_r < 1.05 \end{cases} \tag{6}$$

Here, $K_I$ is the stress intensity factor. Its exponents $s$ and $p$ indicate that $K_I$ is computed, from the secondary or the primary stress respectively. The parameter $\rho_1$ can be calculated using the expression provided in Eq. (7).

$$\rho_1 = 0.1 \cdot \chi^{0.714} - 0.007 \cdot \chi^2 + 3 \cdot 10^{-5} \cdot \chi^5 \tag{7}$$

## FRACTURE ASSESSMENT POINT

### 1. Analytical formulations

This section presents an analytical formulation of the FAP for each crack configuration.

First, the collapse ratio ($L_r$) formulation has been presented in Eq. (5) as the ratio of the applied load $P$ onto the limit load $P_0$. The applied load is the product of the applied stress ($\sigma_{SPE}$, see Eq. (1)) multiplied by the cross-sectional area of the SPE (see Eq. (8)).

$$P = \sigma_{SPE}\left(A_P + A_S\right) \tag{8}$$

where $A_P$ and $A_S$ respectively represent the cross-sectional area of the uncracked plating and stiffener.

The limit load $P_0$ of the SPE is the sum of the individual limit load of the plating and the stiffener. If the individual component does not include cracks, Eq. (9) can provide the limit load expression for this component.

$$P_0 = \sigma_Y A_{P(or\ S)} \tag{9}$$

Anderson [3] provided limit load formulations for a flat plate including an edge crack (see Eq. (10)) and a flat plate including a middle crack (see Eq. (11)).

$$P_{0,EC} = \sigma_Y \left( 1.072 \left( \sqrt{1 + \left( \frac{a_{EC}}{b_{EC}} \right)^2} - \frac{a_{EC}}{b_{EC}} \right) \left( 1 - \frac{a_{EC}}{H} \right) \right) A_S \tag{10}$$

$$P_{0,MC} = \sigma_Y \left(1 - a_{MC}/2W\right) A_P \tag{11}$$

where the uncracked ligament length $b_{EC}$ corresponds to $H$-$a_{EC}$.

The fracture ratio ($K_r$) expression (see Eq. (3)) is related to the longitudinal stress in the cracked component. Thus, Anderson [3] provided load line compliance solutions for a

flat plate including an edge crack and a flat plate including a middle crack. These solutions resulted in expressions of the actual stress in a cracked stiffener ($\sigma_S$ ; see Eq. (12)) and its attached cracked plating ($\sigma_P$ ; see Eq. (13)).

$$\sigma_S = \frac{\Delta E}{L + 4a_{EC}.V_{EC}\frac{a_{EC}}{H}} \tag{12}$$

$$\sigma_P = \frac{\frac{\Delta E}{1-\nu^2}}{L + a_{MC}.V_{MC}\frac{a_{MC}}{2W}} \tag{13}$$

By substituting Eq. (1) into Eqs. (12) and (13), the actual stress in the cracked stiffener and that in its attached cracked plating can be expressed in terms of longitudinal stress in the SPE ($\sigma_{SPE}$) as provided in Eqs. (14) and (15).

$$\sigma_S = \frac{\sigma_{SPE}}{1 + \frac{4a_{EC}.V_{EC}\frac{a_{EC}}{H}}{L}} \tag{14}$$

$$\sigma_P = \frac{\frac{\sigma_{SPE}}{1-\nu^2}}{1 + \frac{a_{MC}.V_{MC}\frac{a_{MC}}{2W}}{L}} \tag{15}$$

Based on the load line compliance solutions provided in [3], Eqs. (16) and (17) can compute cracked member's dimensionless elongation along the centerline, in the case of an edge crack ($V_{EC}$) and that of a middle crack ($V_{MC}$), respectively.

$$V_{EC}\left(\frac{a_{EC}}{H}\right) = \frac{\frac{a_{EC}}{H}}{\left(1-\frac{a_{EC}}{H}\right)^2}\left[0.99 - \frac{a_{EC}}{H}\left(1-\frac{a_{EC}}{H}\right) \times\left(1.3 - 1.2\frac{a_{EC}}{H} + 0.7\left(\frac{a_{EC}}{H}\right)^2\right)\right] \tag{16}$$

$$V_{MC}\left(\frac{a_{MC}}{2W}\right) = -1.071 + 0.25\frac{a_{MC}}{2W} - 0.357\left(\frac{a_{MC}}{2W}\right)^2 + 0.121\left(\frac{a_{MC}}{2W}\right)^3 - 0.047\left(\frac{a_{MC}}{2W}\right)^4 + 0.008\left(\frac{a_{MC}}{2W}\right)^5 - \frac{1.071}{a_{MC}/2W}\ln\left(1-\frac{a_{MC}}{2W}\right) \tag{17}$$

Finally, for each crack configuration (see Fig. 2), the dimensionless functions $Y$ required to evaluate the stress intensity factor (see Eq. (4)) is assessed by FEA as presented in the next section.

## 2. FE-determination of functions Y

The British Standard [8] provides expression for usual dimensionless function $Y$. However, for the middle and edge crack in plates, these expressions do not consider explicitly the stiffness at the side edges due to the presence of attached structural members. This edge stiffness has a significant effect on the stress intensity factor. Therefore, this section extracts dedicated functions $Y$ from FEA of SPEs including cracks. The SPE models consist of quadrilateral shell elements with centered nodes, referenced as S8R5 in Abaqus. The employed material is linear elastic. One end of the SPE is clamped, and a longitudinal uniform displacement ($\Delta$) is imposed on the other end. A spider-web meshing rule is then applied in the crack-tip region, to focus the meshing toward the crack tip. As shown in Fig. 5, this meshing rule produces concentric rings of element centered on the crack tip. Abaqus can then evaluate the stress intensity factor by resolving the J-integrals for every path described by each ring of elements. In addition, the elements in the innermost ring are degenerated to triangles by merging the three nodes of one edge. The kinematic constraint of the crack-tip nodes generates a stress and strain singularity which the shape in $r^{-0.5}$ (with $r$ the distance to the crack tip, see Fig. 5) is compatible with the LEFM problem.

Figs. 6a and 7a show the FE models' geometry used to assess the stress intensity factor at the tip of an edge crack in the stiffener (SPEiEC) and that of a middle crack in the plating

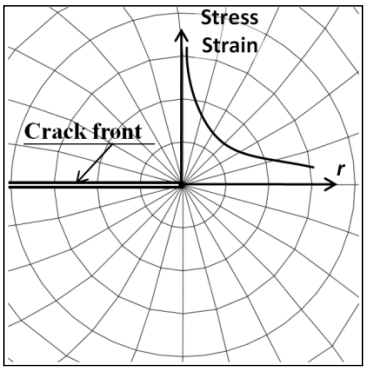


Fig. 5 Spider-web meshing

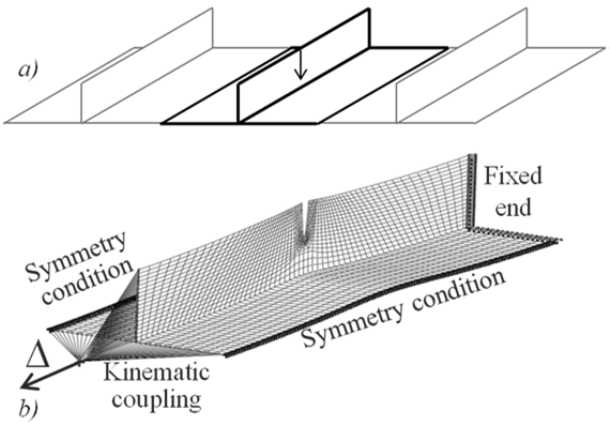


Fig. 6 SPEiEC finite element modeling

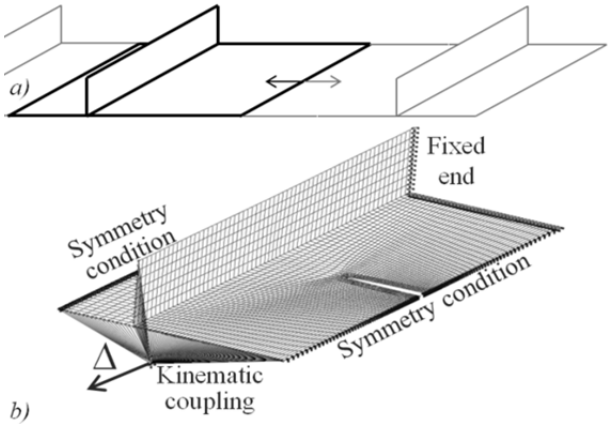


Fig. 7 SPEiMC finite element modeling

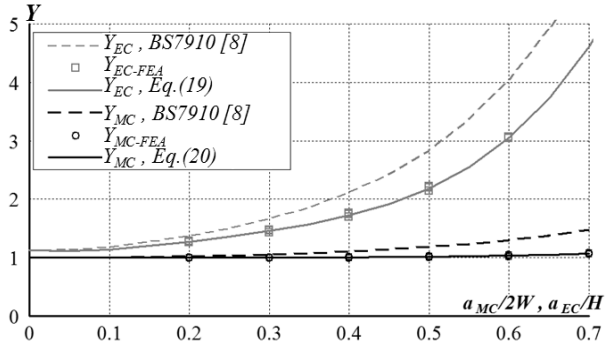


Fig. 8 Function Y evolution for SPEiEC and SPEiMC

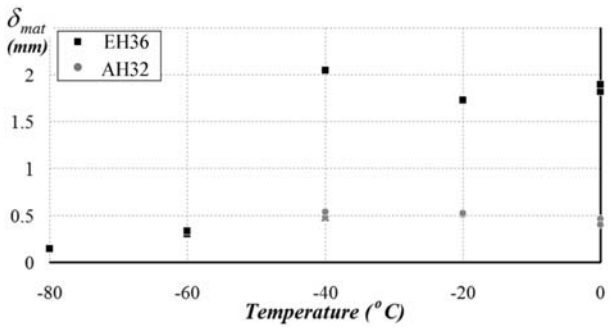


Fig. 9 CTOD measurements

(SPEiMC), respectively. In Figs. 6a and 7a, the structural members represented with thick lines are modelled with finite elements, whereas the effects of the adjacent structural members (thin lines) are considered through symmetry boundary conditions applied to the edges of the finite element model. The stiffener previously cracked in Fig. 6a is not modeled in Fig. 7a since it is supposed to have failed (see Fig. 2b) and thus its influence on the SPE's longitudinal strength is negligible. Figures 6b and 7b also provide a view of the meshing.

For the edge crack configuration (see Fig. 6) and for the middle crack configuration (see Fig. 7), FEA can assess the stress intensity factor ($K_I$) for various crack lengths. These FEAs have been performed for various SPE's plating width ($W$) and stiffener web height ($H$) representative of the considered bulk carrier's midship section scantling.

Table 2 Material fracture toughness

| Steel Grade (-) | Testing temperature (℃) | $\delta_{mat}(mm)$ |
|---|---|---|
| EH36 | -20 | 1.7 |
| AH32 | 0 | 0.4 |

Thus, Eq. (18) can compute the corresponding $Y_{EC\text{-}FEA}$ and $Y_{MC\text{-}FEA}$ using the FEA results $K_{I,EC\text{-}FEA}$ and $K_{I,MC\text{-}FEA}$, respectively.

$$Y_{FEA} = \frac{K_{I,FEA}}{\sigma\sqrt{\pi \cdot a}} \tag{18}$$

where, $a$ corresponds to $a_{EC}$ and $\sigma$ to $\sigma_S$ (see Eq. (14)) for the edge crack configuration, whereas $a$ corresponds to $0.5a_{MC}$ and $\sigma$ to $\sigma_P$ (see Eq. (15)) for the middle crack configuration.

Fig. 8 presents $Y_{EC\text{-}FEA}$ and $Y_{MC\text{-}FEA}$ as extracted using FEA (see Eq. (18)). For each analyzed edge crack length $a_{EC}$ until 60% of the web height and middle crack length $a_{MC}$ until 70% of the plating width, the corresponding $Y_{EC\text{-}FEA}$ and $Y_{MC\text{-}FEA}$ present, at the most, 2% deviations between all the representative dimensions of SPEs. Therefore, general $Y$ formulations capable of evaluating the stress intensity factor of any SPE in the midship section can be fitted to the $Y_{EC\text{-}FEA}$ and $Y_{MC\text{-}FEA}$ values. Eq. (19) can compute $Y_{EC}$ and Eq. (20) can compute $Y_{MC}$. Those expressions are accurate enough for a $K_I$ assessment.

$$Y_{EC}\left(\frac{a_{EC}}{H}\right) = 36.31\left(\frac{a_{EC}}{H}\right)^4 - 31.50\left(\frac{a_{EC}}{H}\right)^3 + 12.45\left(\frac{a_{EC}}{H}\right)^2 - 0.75\frac{a_{EC}}{H} + 1.12 \tag{19}$$

$$Y_{MC}\left(\frac{a_{MC}}{2W}\right) = -0.07\left(\frac{a_{MC}}{2W}\right)^5 + 0.85\left(\frac{a_{MC}}{2W}\right)^4 - 0.62\left(\frac{a_{MC}}{2W}\right)^3 + 0.22\left(\frac{a_{MC}}{2W}\right)^2 - 0.03\frac{a_{MC}}{2W} + 1 \tag{20}$$

In addition, the expressions provided in [8] have been displayed in Fig. 8 for comparison. In that figure, it can be observed that as the cracks get larger the deviations between the handbook formula and the FE results become significant. This comforts the choice to employ FEA to extract dedicated formulations of $Y$.

## 3. Material toughness

The material toughness ($\delta_{mat}$) of the steel grades EH36 and AH32 (see Table 1) were gathered during material type approval conducted by CR. The measurements were performed according to the procedure described in the "Standard

Test Method for CTOD Fracture Toughness Measurement" provided by ASTM E1290 [11]. This test involves a notched specimen in three-points bending condition. The specimens are 50mm square cross-sectional bars. The measurement indicates only the material fracture toughness at the onset of fracture, and ignores the subsequent crack growth resistance behaviour. Fig. 9 presents the results of the CTOD measurement at various testing temperatures.

The FAD Level-2 methodology [8] states that $\delta_{mat}$ is related to the temperature of the structure at which the fracture occurs. Here, the temperature was chosen as the Charpy V-notch (CVN) testing required temperature depicted in class rules [10]. Additionally, the chosen $\delta_{mat}$ was set as the lowest measured value for temperatures ranging from the CVN's temperature to 0°C. Table 2 lists the chosen $\delta_{mat}$. At these temperatures and for both steel grades, the results indicate that the specimen fracture behaviour is ductile.

The results of this test are directly related to the specimen geometry because the stress triaxiality effect at the crack tip increases with the thickness [3]. However, using specimen thicker than any structural members in the ship, the crack-tip condition in the specimen is at least as much severe as the crack-tip condition in the real structure. Therefore, transferring the measured $\delta_{mat}$ to the real structure leads to a conservative assessment of the fracture conditions.

## FRACTURE RESISTANCE

For both crack configurations (see Fig. 2) and for various crack lengths, the applied stress ($\sigma_{SPE}$) corresponding to the failure stress ($\sigma_f$) is assessed in such a manner that the FAP is located on the FAC (see Fig. 3).

Thus, the collapse and fracture ratios can be assessed analytically as a function of $\sigma_{SPE}$ (see Section 3). Tables 1 and 2 list the SPE dimensions and properties, and the material toughness, respectively. For a crack tip distant from the heat affected zone, Dinovitzer et al. [7] considered conservatively a residual stress equal to 20% of the material yield stress. In addition, the residual stress is considered uniform through the thickness and constant across the component.

Figs. 10 and 11 show the failure stress evolution for SPE located in the deck and in the bottom, respectively. Both figures show that for small cracks, the FAP is located on the vertical limit ($L_r$=1) of the FAC that corresponds to the yield strength of the SPE. For larger cracks, the failure occurs then by fracture. To ensure an accurate FAP analytical evaluation, the results are restricted to the validity domain of each dimensionless function $Y_{EC}$ and $Y_{MC}$ (see Eqs. (19) and (20)). Thus, the failure stress is determined until an edge crack length corresponding to 60% of the web height and a middle crack length equals to 70% of the plating width.

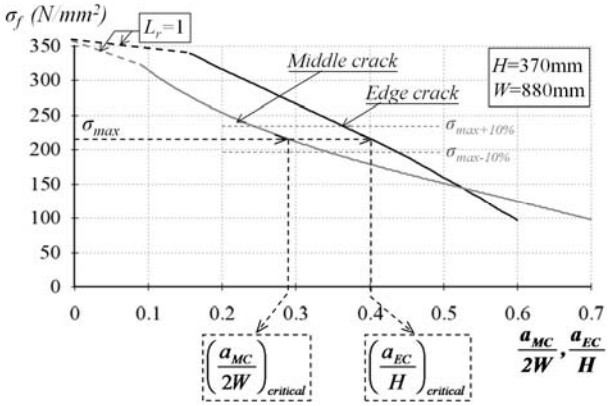


Fig. 10 Failure stress of SPE located in the deck

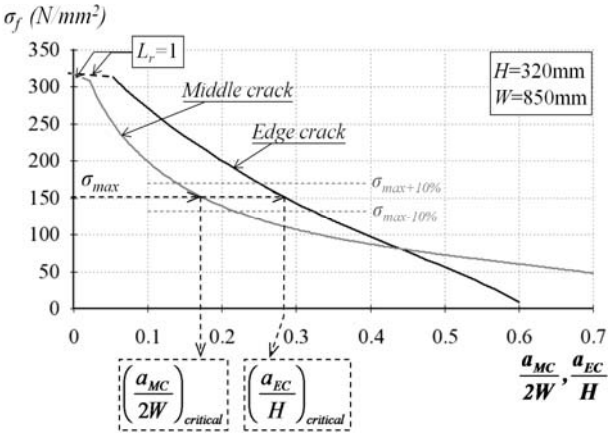


Fig. 11 Failure stress of SPE located in the bottom

Figs. 10 and 11 reveal that the structural member located in the deck has a failure stress significantly higher than the one located in the bottom. This can be explained by the fact that the material in the deck has higher yield stress and toughness than that in the bottom (see Tables 1 and 2). Finally, for the edge fatigue crack considering $L_r \neq 1$, the failure stress decreases quasi-linearly as the crack length increases. For the middle fatigue crack considering $L_r \neq 1$, the failure stress drops rapidly for small cracks, but that decrease becomes slower for large cracks.

Then, for each SPE (see Table 3), the maximum longitudinal stress ($\sigma_{max}$) is evaluated based on the long-term extreme hull girder vertical bending moment provided by the rules [1] which corresponds to a $10^{-8}$ probability level. Table 4 lists the estimated maximum longitudinal stress in the $SPE_{Deck}$ and $SPE_{Bottom}$. For the $SPE_{Deck}$, the bending moment is positive because it corresponds to the hogging condition for which the

Table 3 Maximum longitudinal stress

| SPE location | Maximum hull girder vertical bending moment | Section modulus | Maximum stress |
|---|---|---|---|
| | $M_{v\text{-}max}$ (MN.m) | $Z$ ($m^3$) | $\sigma_{max}$ ($N/mm^2$) |
| Deck | 5078.44 | 23.27 | 218.2 |
| Bottom | -5106.8 | 33.32 | 153.2 |

Table 4 Critical crack length

| SPE location | Edge crack in stiffener $a_{EC,\text{critical}}$ (mm) ($a_{EC,\sigma max\pm10\%}/a_{EC,\sigma max}$) | | | Middle crack in plating $a_{MC,\text{critical}}$ (mm) ($a_{MC,\sigma max\pm10\%}/a_{MC,\sigma max}$) | | |
|---|---|---|---|---|---|---|
| - | $\sigma_{max}$ | $\sigma_{max\text{-}10\%}$ | $\sigma_{max+10\%}$ | $\sigma_{max}$ | $\sigma_{max\text{-}10\%}$ | $\sigma_{max+10\%}$ |
| Deck | 148 (-) | 161 (+9%) | 133 (-10%) | 493 (-) | 598 (+21%) | 422 (-14%) |
| Bottom | 90 (-) | 102 (+13%) | 80 (-11%) | 289 (-) | 365 (+26%) | 238 (-18%) |

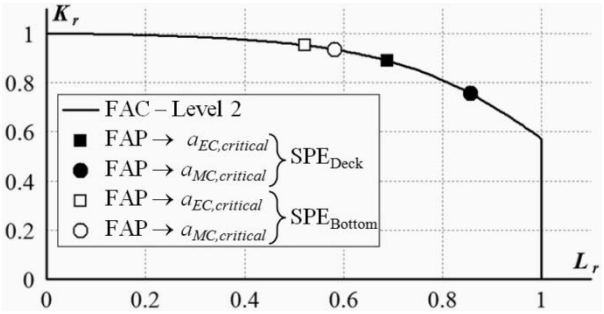


Fig. 12 FAPs of critical crack lengths

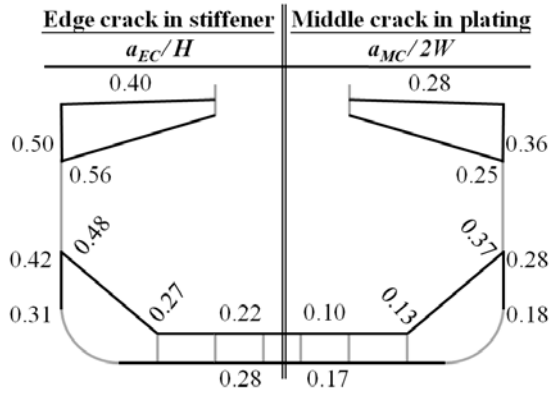


Fig.13 Nondimensional critical crack lengths in the midship section

deck is in tension, whereas for the SPE$_{Bottom}$, the bending moment is negative because it corresponds to the sagging condition for which the bottom is in tension.

According to Figs. 10 and 11, the critical crack lengths can thus be evaluated corresponding to the maximum longitudinal stress ($\sigma_{max}$) defined in Table 3. Table 4 lists the critical fatigue crack lengths. Table 4 reveals that although the applied maximum stress ($\sigma_{max}$) in the bottom is approximately 30% lower than that on the deck, the critical crack lengths for the SPE$_{Bottom}$ are significantly (~30-40%) smaller than that for the SPE$_{Deck}$. It can be concluded that the low material yield stress and toughness in the bottom affects significantly the resistance capacity to fracture of the structural member located in that region. Then, Fig. 12 presents the FAPs location on the FAC for each critical crack length evaluated. As expected, the FAPs are all positioned on the right of the diagram that describes the ductile fracture behaviour (see Fig. 3).

In addition, the critical crack lengths are evaluated for stress level of +10% and -10% of σmax as shown on Figs. 10 and 11. The extracted critical crack lengths are listed and compared to the original values in Table 4. It can be observed that for the edge crack configuration, the critical length variations follow the same magnitude as that of the applied stress. For the middle crack configuration, the critical length variations are comprised between +26% and -18%. Therefore, the maximum longitudinal stress has a larger effect on the fracture resistance of the plating.

The procedure is repeated to every longitudinal member in the midship section. Fig. 13 presents the fracture resistance obtained for both crack configurations. In Fig. 13, it can be observed that the fracture resistance is smaller for the deck and bottom areas than around the neutral axis. Indeed, the maximum stress induced by extreme vertical bending moment becomes negligible at the vertical neutral axis. Then, low levels of critical crack length are found in the inner bottom. Those members are made of mild steel and since no $\delta_{mat}$ data were available for the steel grade A, this study employed that from the AH32. However, since the mild steel is much lowly alloyed than AH32 high strength steel, its toughness should be higher, and higher fracture resistance can thus be expected for the inner bottom.

## CONCLUSION

This study evaluates the critical fatigue crack length of ship longitudinal members considering the fracture failure of those members including fatigue crack. Specifically, this study adopts the Failure Assessment Diagram (FAD) methodology to assess the condition of fracture failure at the tip of two crack configurations. This study establishes the analytical formulations of the crack-tip conditions that are validated using finite element analyses.

First, for each crack configurations, the failure stress evolutions are assessed as a function of the fatigue crack length. Then, the critical crack lengths are evaluated as they

relate to a maximum axial stress derived from the long-term extreme hull girder vertical bending moments:

- For a single edge crack initiating from the free edge of a flat bar stiffener, the critical edge crack length corresponds to approximately 40% of the web height for a stiffener located in the deck and 28% for a stiffener located in the bottom.
- For a single middle crack initiating from the fillet weld at the connection with the stiffener, the critical middle crack length corresponds to approximately 28% of the plating width for a panel located in the deck and 17% for a panel located in the bottom.

The fracture resistance is then evaluated for every longitudinal member in the midship area. As a result, the fracture resistance of the bottom components is confirmed to be smaller than that for deck components. For longitudinal members closer to the vertical neutral axis, the fracture resistance increases, since the maximum stress decreases. For the whole ship section, the critical fatigue crack lengths are very large, so that the fracture resistance is satisfactory.

Therefore, this study shows that for typical cracked longitudinal members, the ordinary ship design and fabrication provide sufficient redundancy against fracture to the cracked structure.

Finally, this study shows practically how a simplified approach to assess the fracture resistance at the onset of fracture is perfectly adapted to this case of study. Once the analytical formulations are established for the specific case of longitudinal members including cracks, the computations are very fast and can be repeated to many dimensions of longitudinal stiffener. However, in the case of fracture analyses taking into account the crack propagation in complicated geometry, finer numerical methods that include detailed material fracture behaviour should be preferred.

## NOMENCLATURE

**English symbols**

| | |
|---|---|
| $a_{EC}$,$a_{MC}$ | Edge crack and middle crack lengths |
| $A_P$, $A_S$ | Cross sectional area of the plating and stiffener of a SPE |
| $K_I$ | Mode I stress intensity factor |
| $K_r$ | Fracture ratio |
| $L_r$ | Collapse ratio |
| $M_{v\text{-max}}$ | Maximum hull girder vertical bending moment |
| $P$ | Applied load |
| $P_0$ | Limit load |
| $Y$ | Dimensionless function (see Eq. (4)) |

**Greek symbols**

| | |
|---|---|
| $\Delta$ | Structural member's longitudinal displacement |
| $\delta_{mat}$ | Material toughness, crack-tip opening displacement (CTOD) |
| $\sigma_f$ | Failure stress |
| $\sigma_{\max}$ | Maximum stress |
| $\sigma_P$, $\sigma_S$ | Actual stresses in the cracked plating and stiffener |
| $\sigma_{SPE}$ | Applied longitudinal stress in the SPE |

## REFERENCES


1. CSR-H, "*Common Structural Rules for Bulk Carriers and Oil Tankers*," IACS (2013).
2. IMO, Adoption of the International Goal-Based Ship Construction Standard for Bulk Carriers and Oil Tankers, MSC. 290 (87), Maritime Safety Committee (MSC) (2010).
3. Anderson, T.L., "*Fracture Mechanics - Fundamentals and Applications*," Taylor & Francis, Boca Raton (2005).
4. Gurson, A.L., *"Plastic Flow and Fracture Behaviour of Ductile Materials Incorporating Void Nucleation, Growth and Coalescence,"* PhD Diss., Brown university, (1975).
5. Thomason, P.F., *Ductile Fracture of Metals*, Pergamon Press, Oxford (1990).
6. Zhang, Z.L., *"A Complete Gurson Model Approach for Ductile Fracture*," Engineering Fracture Mechanics, Vol.67, pp.155-168 (2000).
7. Dinovitzer, A.S. and Pussegoda, N., *"Fracture Toughness of a Ship Structure*," SSC-430, Ship Structure Committee (SSC), Washington DC (2003).
8. BS7910, *"Guide to Methods for Assessing the Acceptability of Flaws in Metallic Structures*," British Standard Institute (BSI) (2005).
9. SINTAP, *Structural Integrity Assessment Procedure*, FITNET (1999).
10. CR, *"Rules for the Construction and Classification of Steel Ships*," China Corporation Register of Shipping (CR) (2009).
11. ASTM E1290, Standard Test Method for Crack-Tip Opening Displacement (CTOD) Fracture Toughness Measurement, American Society for Testing and Material, (2010).

# 船舶結構破壞抗力評估簡化方法

吳 凱 洋　　黃 建 樺　　李 綺 芳

財團法人中國驗船中心 研究處

關鍵詞：破壞、縱向構件、破壞評估圖、裂縫開口位移

## 摘　　要

本研究探討具有疲勞裂縫之船舶縱向構件的破壞失效問題。船的一生中遭遇極端海況時，部分疲勞裂縫可能成長達到一臨界長度進而造成迅速破壞。臨界裂縫長度之大小可表現結構對於破壞之抵抗能力。本研究提出一簡化法以求取此臨界裂縫長度，所採用之方法為破壞評估圖，其可用來評估裂縫尖端之破壞狀況。本研究為兩種不同型式之裂縫，以有限元素分析法回歸出裂縫尖端狀況之解析化公式，並將材料韌性以裂縫尖端開口位移來表示。此簡化法可快速計算具有裂縫之縱向構件的破壞應力，將破壞應力表示為裂縫長度之函數。再將長期極端負荷下所造成之最大縱向應力代入，即可得到臨界裂縫長度。本研究以一艘海岬型散裝船為例，發現其裂縫臨界長度很大，破壞抗力良好。

(Manuscript received Jan. 15, 2014,
Accepted for publication Mar. 13, 2014)